nature communications

Article

https://doi.org/10.1038/s41467-024-52689-5

SARS-CoV-2 spike-specific nasal-resident CD49a$^+$CD8$^+$ memory T cells exert immediate effector functions with enhanced IFN-γ production

Received: 4 November 2023

Accepted: 19 September 2024

Published online: 27 September 2024

Check for updates

Min-Seok Rha[1,2], Gyeongyeob Kim[1], Sol Lee[1], Jihye Kim[3], Yeonsu Jeong[1], Chan Min Jung[1], Hae Eun Noh[1], Ji Yun Noh[4], Yong Min Kim[5,6], Hyung-Ju Cho[1,2], Chang-Hoon Kim[1,2] ✉ & Eui-Cheol Shin[3,7] ✉

Virus-specific nasal resident T cells are important for protection against subsequent infection with a similar virus. Here we examine the phenotypes and functions of SARS-CoV-2-specific T cells in the nasal mucosa of vaccinated individuals with breakthrough infection (BTI) or without infection. Nasal tissues are obtained from participants during sinus surgery. Analysis of activation-induced markers implicates that a considerable proportion of spike (S)-reactive nasal CD8$^+$ T cells express CD103, a tissue-resident marker. MHC-I multimer staining is performed to analyze the ex vivo phenotype and function of SARS-CoV-2 S-specific CD8$^+$ T cells. We detect multimer$^+$CD8$^+$ T cells with tissue-resident phenotypes in nasal tissue samples from vaccinees without infection as well as vaccinees with BTI. Multimer$^+$CD8$^+$ T cells remain present in nasal tissues over one year after the last exposure to S antigen, although the frequency decreases. Upon direct ex vivo stimulation with epitope peptides, nasal multimer$^+$CD8$^+$ T cells–particularly the CD49a$^+$ subset–exhibit immediate effector functions, including IFN-γ production. CITE-seq analysis of S-reactive AIM$^+$CD8$^+$ T cells confirms the enhanced effector function of the CD49a$^+$ subset. These findings indicate that among individuals previously exposed to S antigen by vaccination or BTI, S-specific nasal-resident CD49a$^+$CD8$^+$ memory T cells can rapidly respond to SARS-CoV-2 during infection or reinfection.

Memory T cells can be elicited by natural infection with severe acute respiratory syndrome coronavirus 2 (SARS-CoV-2) or vaccination[1–5]. Accumulating evidence suggests that memory T-cell responses play critical roles in protecting against severe coronavirus disease 2019 (COVID-19), particularly when facing SARS-CoV-2 variants that escape the neutralizing activities of vaccine-induced antibodies[6–9]. A better understanding of memory T-cell responses following natural infection or vaccination will help guide the development of next-generation vaccines against COVID-19 and other viral diseases.

Tissue-resident memory T (T_{RM}) cells act as front-line defenders against invading pathogens in barrier tissues[10–12]. T_{RM} cells are present in the upper and lower respiratory tracts, including in nasal and lung mucosal tissues. In influenza virus-infected hosts, nasal CD8$^+$ T_{RM} cells limit viral spread and reduce disease severity[13], and the intranasal transfer of CD8$^+$ T_{RM} cells can confer protection against respiratory

A full list of affiliations appears at the end of the paper. ✉e-mail: entman@yuhs.ac; ecshin@kaist.ac.kr

syncytial virus infection[14]. In mouse models of coronavirus infection, IFN-γ produced by airway $CD4^+$ T_{RM} cells is a main mediator of protection[15]. Since nasal mucosa is the primary site of entry and initial SARS-CoV-2 replication[16], nasal T_{RM} cells are likely to be early responders upon SARS-CoV-2 exposure. However, most previous analyses of T-cell responses against SARS-CoV-2 have been limited to peripheral blood (PB).

Following COVID-19 resolution, SARS-CoV-2-specific T_{RM} cells are detected in the nasal cavity, bone marrow, spleen, and lungs[17,18]. However, it remains unclear whether COVID-19 vaccination induces SARS-CoV-2 spike (S)-specific T_{RM} cells in the airway. One study found S-specific T cells in nasopharyngeal swab samples from vaccinees[19], supporting recent findings that mRNA vaccination induced T_{RM}-cell generation in a murine model[20]. In contrast, other studies have detected S-specific T-cell responses in nasal secretions or bronchoalveolar lavage fluid (BALF) samples from vaccinees who experienced breakthrough infections (BTI), but not from vaccinees without infection[21,22]. In a recent study, BALF was evaluated after immunization or infection, revealing that vaccination without infection did not induce significantly greater S-specific T-cell responses compared to in prepandemic samples[23]. Since Omicron variants preferentially replicate in the nasal mucosa[24], it is critical to examine T_{RM} cells in nasal mucosa tissues. However, previous studies have analyzed nasal swab, secretion, or curettage samples, which do not exactly represent the nasal mucosa tissue, and may contain only the T cells located in the epithelium[18,21]. Analysis of nasal mucosa tissues is required to improve our understanding of the detailed phenotype and function of nasal SARS-CoV-2-specific T_{RM} cells.

Notably, prior studies have detected SARS-CoV-2 S-specific T_{RM} cells using activation-induced marker (AIM) assays, IFN-γ ELISpot assays, or intracellular cytokine staining following in vitro stimulation with overlapping peptides (OLPs). Stimulation-based assays using OLPs covering the SARS-CoV-2 S protein can detect not only SARS-CoV-2 S-specific T cells but also pre-existing cross-reactive T cells that may have been originally primed by common cold coronaviruses (CCCoVs) or animal CoVs[25–28]. Although cross-reactive T cells may participate in immune responses upon infection, there remains a need to investigate bona fide SARS-CoV-2-specific T cells in nasal mucosa tissues. Using MHC-I multimers loaded with SARS-CoV-2 S-specific epitope peptides that have a low degree of homology to CCCoVs[29] increases the likelihood of excluding T cells cross-reactive to other pathogens.

In the present study, we examine the frequencies and phenotypes of S-reactive AIM^+ T cells in nasal tissues from vaccinees with BTI or without infection. We also investigate the frequencies and tissue-resident phenotypes of S-specific MHC-I $multimer^+CD8^+$ T cells in nasal tissues. We find S-specific MHC-I $multimer^+CD8^+$ T cells that exhibit tissue-resident phenotypes in nasal mucosa tissues from vaccinees without infection as well as vaccinees with BTI. Furthermore, we demonstrate that nasal-resident S-specific $multimer^+CD8^+$ T cells expressing CD49a rapidly respond to epitope peptides by producing IFN-γ, indicating their immediate effector functions.

Results

Study cohort and nasal T-cell phenotypes

For this study, we acquired PB and nasal tissues from patients who underwent endoscopic sinus surgery (ESS) and obtained PB mononuclear cells (PBMCs) and nasal cells. The enrolled patients were categorized into two groups according to their vaccination and infection history: vaccinees without previous infection or BTI (vaccinated group) and vaccinees who experienced BTI (BTI group). To confirm the absence of infection either before or after vaccination for the vaccinated group, we performed plasma anti-nucleocapsid (N) antibody assays. We also analyzed nasal cells that had been cryopreserved before the onset of the COVID-19 pandemic (unexposed group). To evaluate the phenotypes of S-specific nasal T cells from the unexposed, vaccinated, and BTI groups, we conducted AIM assays and MHC-I multimer staining (Fig. 1a). Supplementary Table 1 presents the demographic and clinical characteristics of the enrolled patients.

We first compared the ex vivo phenotypes of total $CD8^+$ and $CD4^+$ T cells in paired samples of PBMCs and nasal cells (Supplementary Fig. 1). We evaluated T_{RM} features by analyzing data from all three groups together. We examined the expressions of CD69 and CD103, which are canonical markers of T_{RM} cells[10,11], and found that the frequencies of $CD69^+CD103^+$ and $CD69^+CD103^-$ cells among total $CD8^+$ T cells were significantly higher in nasal tissue than in PB (Fig. 1b). The same results were observed among total $CD4^+$ T cells (Fig. 1b). We also assessed the expression of CD49a (integrin α1), another marker of epithelial tissue T_{RM} cells[11], and CXCR6, an airway-homing chemokine receptor[30]. The percentages of $CD49a^+$ and $CXCR6^+$ cells were significantly higher among $CD69^+CD103^+$ or $CD69^+CD103^-$ $CD8^+$ T cells, compared to among $CD69^-CD103^-$ $CD8^+$ T cells (Fig. 1c), confirming the tissue-resident feature of $CD69^+CD103^+$ and $CD69^+CD103^-$ nasal $CD8^+$ T cells. Analysis of nasal $CD4^+$ T cells revealed similar findings (Fig. 1c). The expression patterns of T_{RM} markers on nasal $CD8^+$ and $CD4^+$ T cells were presented as t-SNE plots (Supplementary Fig. 2). The frequencies of $CD69^+CD103^+$ and $CD69^+CD103^-$ cells among nasal $CD8^+$ and $CD4^+$ T cells did not significantly differ between the unexposed, vaccinated, and BTI groups (Fig. 1d). These patient groups also did not significantly differ in the percentages of $CD49a^+$ and $CXCR6^+$ cells among nasal $CD8^+$ and $CD4^+$ T cells (Fig. 1e). Nasal $CD8^+$ T cells predominantly comprised of $CD69^+$ T_{RM} cells and $CCR7^-CD45RA^-$ effector memory (T_{EM}) cells, with only ~2% being $CCR7^-CD45RA^+$ terminally differentiated effector memory (T_{EMRA}) cells (Fig. 1f). The majority (~87%) of nasal $CD4^+$ T cells were $CD69^+$ T_{RM} cells and $CCR7^-CD45RA^-$ T_{EM} cells, while ~10% were $CCR7^+CD45RA^-$ central memory (T_{CM}) cells (Fig. 1f). Overall, these results indicate an enrichment of T_{RM} cells in the nasal tissue.

S-reactive AIM+ cells are detected among nasal T cells

We next analyzed S-reactive nasal T cells by performing AIM assays[31,32] after S OLP stimulation of nasal cells obtained from unexposed, vaccinated, and BTI groups. $CD25^+CD137^+$ cells and $OX40^+CD137^+$ cells were considered S-reactive AIM^+ cells among $CD8^+$ and $CD4^+$ T cells, respectively (Fig. 2a)[17]. S-reactive AIM^+ cells were detected among $CD8^+$ and $CD4^+$ T cells in all three patient groups. However, the frequencies of AIM^+ cells among $CD8^+$ and $CD4^+$ T-cell populations were significantly higher in the vaccinated and BTI groups, compared to in the unexposed group (Figs. 2b, c). We performed AIM assays after N OLP stimulation, and found that the frequencies of AIM^+ T cells among $CD4^+$ and $CD8^+$ T cells were significantly higher in the BTI group than in the unexposed and vaccinated groups, and did not differ between the unexposed and vaccinated groups (Supplementary Fig. 3). The similar levels of T-cell responses against SARS-CoV-2 N protein between the vaccinated and unexposed groups strongly support the absence of infection history in the vaccinated group.

We further analyzed the percentages of positive responders in the AIM assays. A positive response was defined as when the percentage of AIM^+ cells after S OLP stimulation was at least three-fold higher than that of negative controls. In our analysis of $CD8^+$ T cells, AIM responses were observed in 28.2% (11 of 39) of the unexposed group, compared to 69.0% (29 of 42) of the vaccinated group, and 75.0% (15 of 20) of the BTI group (Fig. 2d). Our analysis of $CD4^+$ T cells revealed AIM responses in 48.7% (19 of 39) of the unexposed group, 64.3% (27 of 42) of the vaccinated group, and 75.0% (15 of 20) of the BTI group (Fig. 2e).

The vaccinated and BTI groups exhibited higher frequencies of S-reactive AIM^+ T cells and percentages of AIM responders compared to the unexposed group. However, a considerable proportion of unexposed individuals had S-reactive AIM^+ cells in their nasal tissues.

https://doi.org/10.1038/s41467-024-52689-5

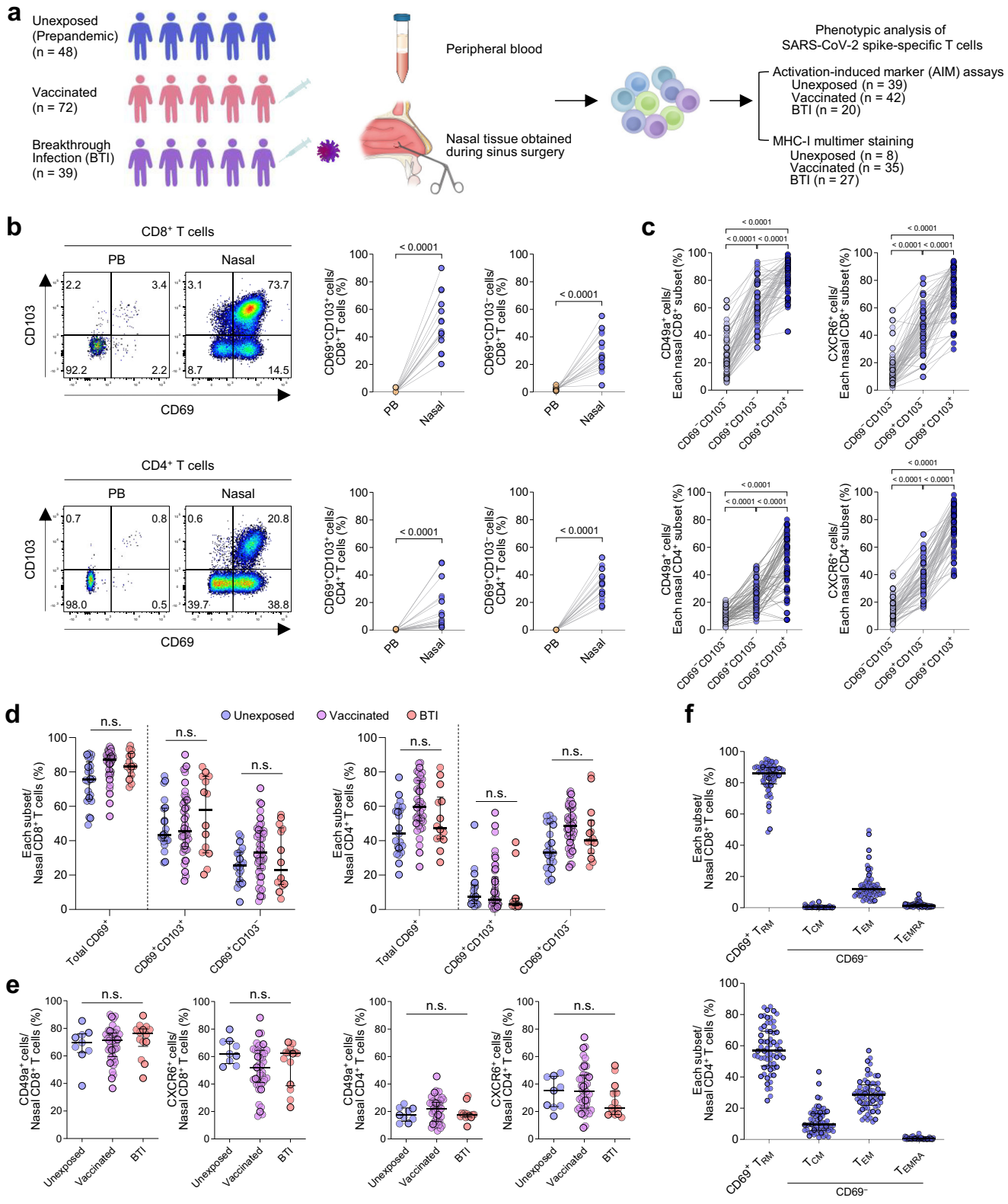

Fig. 1 | Phenotypic analysis of nasal T cells. a Study scheme for analysis of SARS-CoV-2 S-specific T cells in peripheral blood (PB) and nasal tissue from three patient groups: unexposed (prepandemic), vaccinated (vaccinees without infection) and BTI (vaccinees with BTI). **b** Representative flow cytometry plots and summary data for the frequencies of $CD69^+CD103^+$ and $CD69^+CD103^-$ cells among $CD8^+$ and $CD4^+$ T cells from paired PBMC and nasal cell samples ($n = 16$). **c** Frequencies of $CD49a^+$ and $CXCR6^+$ cells among the indicated nasal T-cell subsets ($n = 64$). **d,e**, Frequencies of total $CD69^+$ (**d**) $CD69^+CD103^+$ (**d**), $CD69^+CD103^-$ (**d**), $CD49a^+$ (**e**), and $CXCR6^+$ (**e**) cells among nasal $CD8^+$ or $CD4^+$ T cells from the unexposed (**d** $n = 21$; **e** $n = 9$), vaccinated (**d** $n = 42$; **e** $n = 42$), and BTI (**d** $n = 14$; **e** $n = 14$) patient groups. **f** Frequencies of $CD69^+$ T_{RM}, $CD69^-CCR7^-CD45RA^-$ (T_{EM}), $CD69^-CCR7^+CD45RA^-$ (T_{CM}), and $CD69^-CCR7^-CD45RA^+$ (T_{EMRA}) cells among nasal $CD8^+$ or $CD4^+$ T cells ($n = 64$). Data are presented as median and interquartile range. Statistical analysis was performed using the two-tailed Wilcoxon signed-rank test (**b**), one-way repeated-measures ANOVA with Tukey's multiple comparisons test (**c**), or Kruskal-Wallis test with Dunn's multiple comparisons test (**d**, **e**). n.s., not significant. Source data are provided as a Source Data file.

https://doi.org/10.1038/s41467-024-52689-5

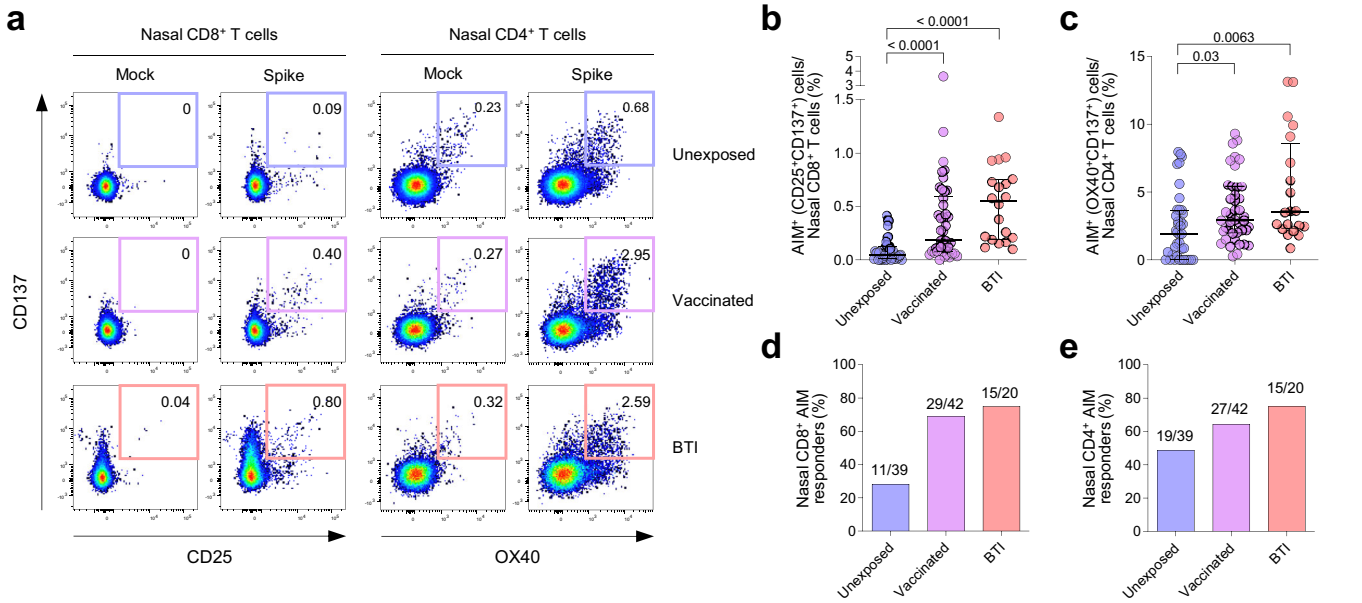

Fig. 2 | Detection of SARS-CoV-2 S-reactive nasal T cells by AIM assays. a–d Nasal cells from unexposed individuals ($n = 39$), vaccinees without infection ($n = 42$), and vaccinees with BTI ($n = 20$) were stimulated with S OLPs for 24 hours, and analyzed by flow cytometry. **a** Representative flow cytometry plots for AIM assays. **b**, **c** The frequencies of S-specific AIM$^+$ cells among CD8$^+$ (**b**) and CD4$^+$ (**c**) T cells, compared among the patient groups. Data are presented as median and interquartile range. **d**, **e** The percentages of positive AIM responders in each patient group, from the analysis of CD8$^+$ (**d**) and CD4$^+$ (**e**) T cells. A positive response was defined as when the percentage of AIM$^+$ cells after OLP stimulation was more than three-fold higher than the percentage of AIM$^+$ cells in the negative controls. Statistical analysis was performed using the Kruskal-Wallis test with Dunn's multiple comparisons test (**b**, **c**). Source data are provided as a Source Data file.

This suggests that S-reactive AIM$^+$ cells could be elicited not only by SARS-CoV-2 infection or vaccination but also by previous infections with cross-reactive pathogens, such as CCCoVs and animal CoVs[25–28]. We also analyzed correlations between the frequencies of S-reactive AIM$^+$ T cells between nasal tissues and PB. The frequency of S-reactive AIM$^+$ T cells among CD8$^+$ T cells in the nasal tissue did not correlate with their frequency in PB while a significant correlation was observed in the analysis of AIM$^+$CD4$^+$ T cells (Supplementary Fig. 4). Furthermore, we investigated possible correlations between the frequency of nasal S-reactive AIM$^+$ T cells and the time since last exposure. This analysis revealed that the frequencies of AIM$^+$CD8$^+$ and AIM$^+$CD4$^+$ T cells were not significantly correlated with the time since last exposure, either by vaccination or infection (Supplementary Fig. 5).

Next, we examined the tissue-resident phenotypes of S-reactive AIM$^+$ cells, and compared these phenotypes among patient groups (Fig. 3a). We did not analyze CD69 expression, because its expression is upregulated following stimulation in AIM assays. In all patient groups, we observed 45–50% average frequencies of CD103$^+$ cells among nasal AIM$^+$CD8$^+$ T cells, without significant differences among patient groups (Fig. 3b). Similarly, the patient groups did not significantly differ in the frequencies of CD103$^+$ cells among nasal AIM$^+$CD4$^+$ T cells (Fig. 3c). Our analysis of differentiation status revealed that nasal AIM$^+$CD8$^+$ T cells were predominantly CCR7$^-$CD45RA$^-$ T_{EM} cells (Fig. 3d). Nasal AIM$^+$CD4$^+$ T cells mainly comprised of CCR7$^-$CD45RA$^-$ T_{EM} cells (~60%) and CCR7$^+$CD45RA$^-$ T_{CM} cells (~40%). Patient groups did not significantly differ in the proportions of each memory subset among nasal AIM$^+$CD8$^+$ or AIM$^+$CD4$^+$ T cells.

S-specific CD8$^+$ T_{RM} cells are present in nasal tissues from both vaccinees with BTI and vaccinees without infection

To examine ex vivo phenotypes of nasal S-specific CD8$^+$ T cells, we next performed direct ex vivo MHC-I multimer staining, using an HLA-A*0201 multimer loaded with SARS-CoV-2 S_{269} (YLQPRTFLL) peptide. This epitope peptide exhibits a low degree of sequence homology (0% to 44%) with CCCoVs[29]. We also used an HLA-A*2402 multimer loaded with SARS-CoV-2 S_{448} (NYNYLYRLF) peptide, which has sequence homology ranging from 0% to 55% with CCCoVs[33]. MHC-I multimer$^+$ cells were detected in nasal tissue samples from both vaccinated and BTI groups (Fig. 4a, Supplementary Fig. 6a), and the frequency of multimer$^+$ cells among nasal CD8$^+$ T cells did not significantly differ between these two groups (Fig. 4b). However, multimer$^+$ cells were not detected in nasal tissue samples from the unexposed group (Figs. 4a, b). We further validated the absence of multimer$^+$ cells in the nasal tissue samples of unexposed individuals by generating primary T cell lines stimulated with epitope peptides for 7 days (Supplementary Fig. 6b). Additionally, AIM$^+$ cells were not detected among nasal cells from the unexposed group upon ex vivo epitope peptide stimulation (Supplementary Fig. 6c).

We next analyzed the expression of tissue-resident markers among nasal multimer$^+$ cells from vaccinated and BTI groups. Among nasal multimer$^+$ cells, we found average proportions of approximately 60% CD69$^+$ cells, 15% CD69$^+$CD103$^+$ cells, and 45% CD69$^+$CD103$^-$ cells in both the vaccinated and BTI groups, with no significant differences between these patient groups (Fig. 4c). Additionally, we found average proportions of approximately 70% CD49a$^+$ and 40% CXCR6$^+$ cells among nasal multimer$^+$ cells, which did not significantly differ between the vaccinated and BTI groups (Fig. 4d). Notably, we confirmed that CD69$^+$CD103$^+$ and CD69$^+$CD103$^-$ cells were observed exclusively among multimer$^+$ cells from the nasal tissue, not from PB (Fig. 4e). Similarly, CD49a$^+$ and CXCR6$^+$ cells were observed almost exclusively among multimer$^+$ cells from the nasal tissue (Fig. 4f). The frequency of S-specific MHC-I multimer$^+$CD8$^+$ T cells in PB was not correlated with that in nasal tissue (Supplementary Fig. 7). We also found that the majority (~70% on average) of nasal multimer$^+$ cells were CCR7$^-$CD45RA$^-$ T_{EM} cells, regardless of patient group (Fig. 4g). Overall, our results demonstrate the presence of S-specific CD8$^+$ T_{RM} cells in nasal tissues from both vaccinees with BTI and vaccinees without infection, supporting a recent report that mRNA vaccination can generate airway T_{RM} cells in a murine model[20].

We also analyzed the correlation between the frequency of nasal multimer$^+$ cells and time since the last exposure to the S antigen either

https://doi.org/10.1038/s41467-024-52689-5

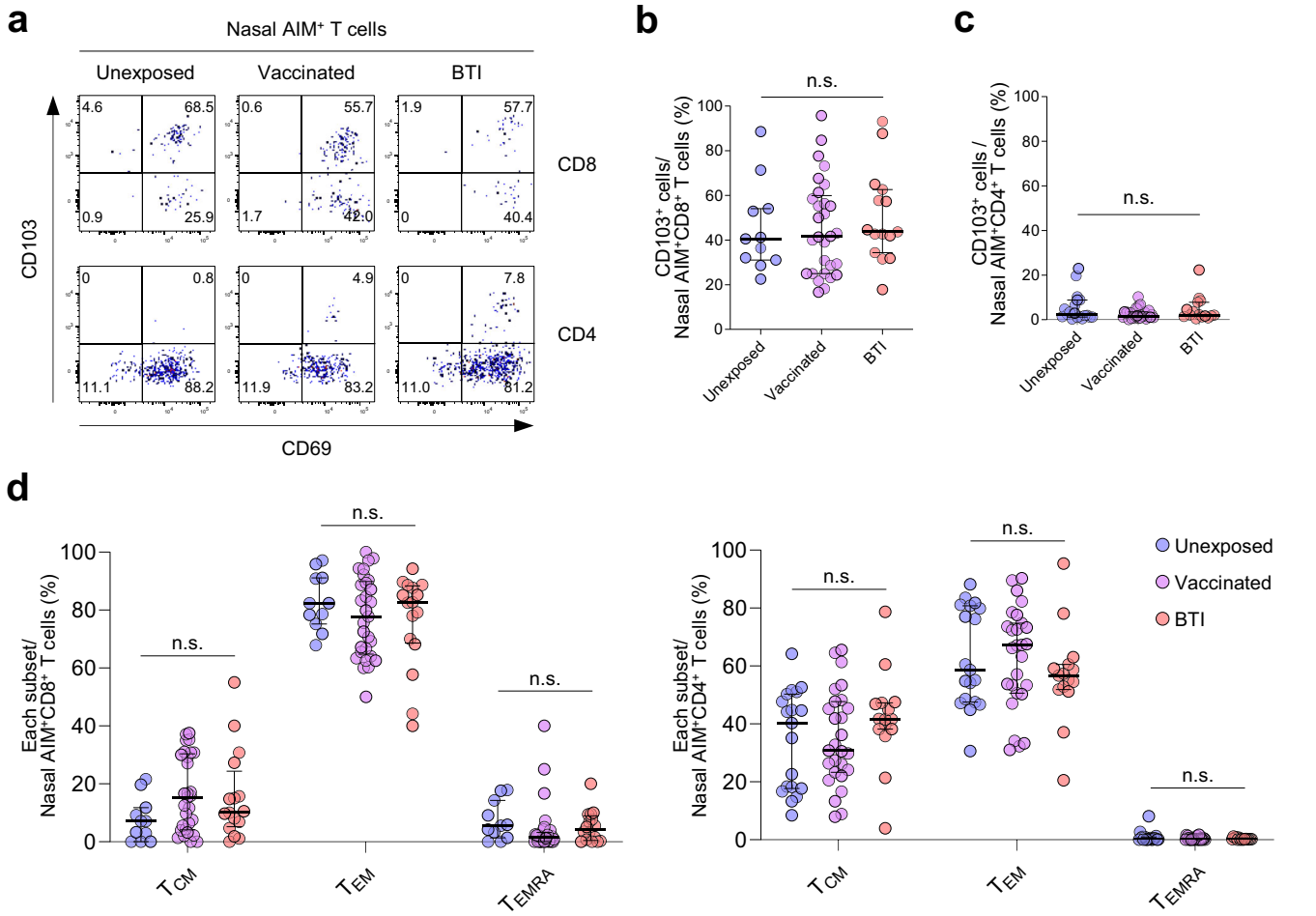

Fig. 3 | Phenotypes of S-reactive nasal AIM⁺ T cells. a–d Phenotypes of S-reactive AIM⁺CD8⁺ T cells (unexposed, $n = 11$; vaccinated, $n = 29$; BTI, $n = 15$) and AIM⁺CD4⁺ T cells (unexposed, $n = 19$; vaccinated, $n = 27$; BTI, $n = 15$). **a–c** Representative flow cytometry plots (**a**) and summary data showing the frequencies of CD103⁺ cells among AIM⁺CD8⁺ (**b**) and AIM⁺CD4⁺ (**c**) T cells. **d** The percentages of CCR7⁻CD45RA⁻ (T_{EM}), CCR7⁺CD45RA⁻ (T_{CM}), and CCR7⁻CD45RA⁺ (T_{EMRA}) cells among AIM⁺CD8⁺ and AIM⁺CD4⁺ T cells. Data are presented as median and interquartile range. Statistical analysis was performed using the Kruskal-Wallis test with Dunn's multiple comparisons test (**b–d**). n.s., not significant. Source data are provided as a Source Data file.

through vaccination or BTI. A significant inverse correlation was observed, with the frequency decreasing over time; however, nasal multimer⁺ cells still remained detectable for over one year after vaccination or BTI (Fig. 4h). These results indicate that S-specific CD8⁺ T cells in the nasal tissue decrease but remain present for a long time following vaccination or BTI.

S-specific nasal MHC-I multimer⁺CD8⁺ T cells exert immediate effector functions upon antigen encounter

A cardinal feature of T_{RM} cells is immediate effector function upon encountering cognate antigens. Therefore, we investigated IFN-γ production by nasal MHC-I multimer⁺ cells. Nasal cells from vaccinated and BTI groups were first stained with S_{269} or S_{448} MHC-I multimers and stimulated with a corresponding peptide (S_{269}, YLQPRTFLL; or S_{448}, NYNYLYRLF) ex vivo for 5.5 hours. We then performed cytokine secretion assays and further staining with MHC-I multimers, for simultaneous analysis of the phenotype and function of multimer⁺ cells[29,34]. Upon epitope peptide stimulation, we detected IFN-γ production by nasal multimer⁺ cells from both the vaccinated (10.7–38.9%) and BTI (7.1–33.0%) groups, with no significant difference between these groups (Figs. 5a, b). This indicates that S-specific nasal CD8⁺ T cells from both vaccinees with BTI and vaccinees without infection rapidly produce an antiviral cytokine upon recognition of cognate antigens.

We next analyzed the IFN-γ-producing capacity of nasal multimer⁺CD8⁺ T cells according to the expressions of T_{RM} markers, including CD103, CD49a, and CXCR6. CD49a⁺ cells exhibited significantly higher IFN-γ production than CD49a⁻ cells, while this difference was not observed between CD103⁺ versus CD103⁻ cells, or CXCR6⁺ versus CXCR6⁻ cells (Fig. 5c, d). We did not perform this comparison between CD69⁺ versus CD69⁻ cells because epitope peptide stimulation rapidly upregulated the expression of CD69 (Supplementary Fig. 8).

Upon epitope peptide stimulation, we also observed degranulation by nasal multimer⁺ cells from both the vaccinated and BTI groups (Fig. 5e), and the frequency of CD107a⁺ cells among nasal multimer⁺CD8⁺ T cells did not significantly differ between these two groups. Additionally, CellTrace Violet (CTV) dilution assays revealed that nasal multimer⁺ cells exhibited robust proliferation following ex vivo stimulation with epitope peptide, with no statistical difference between the patient groups (Fig. 5f). Altogether, these findings demonstrate that vaccination or BTI elicited S-specific nasal CD8⁺ T_{RM} cells capable of proliferating and exerting immediate effector functions upon exposure to cognate antigens. Within the SARS-CoV-2-specific multimer⁺CD8⁺ T-cell population, the frequency of CD107a⁺ cells tended to be higher among CD49a⁺ cells compared to CD49a⁻ cells, although this difference was not statistically significant ($P = 0.083$; Supplementary Fig. 9a). The frequency of CTV^{low} cells did

https://doi.org/10.1038/s41467-024-52689-5

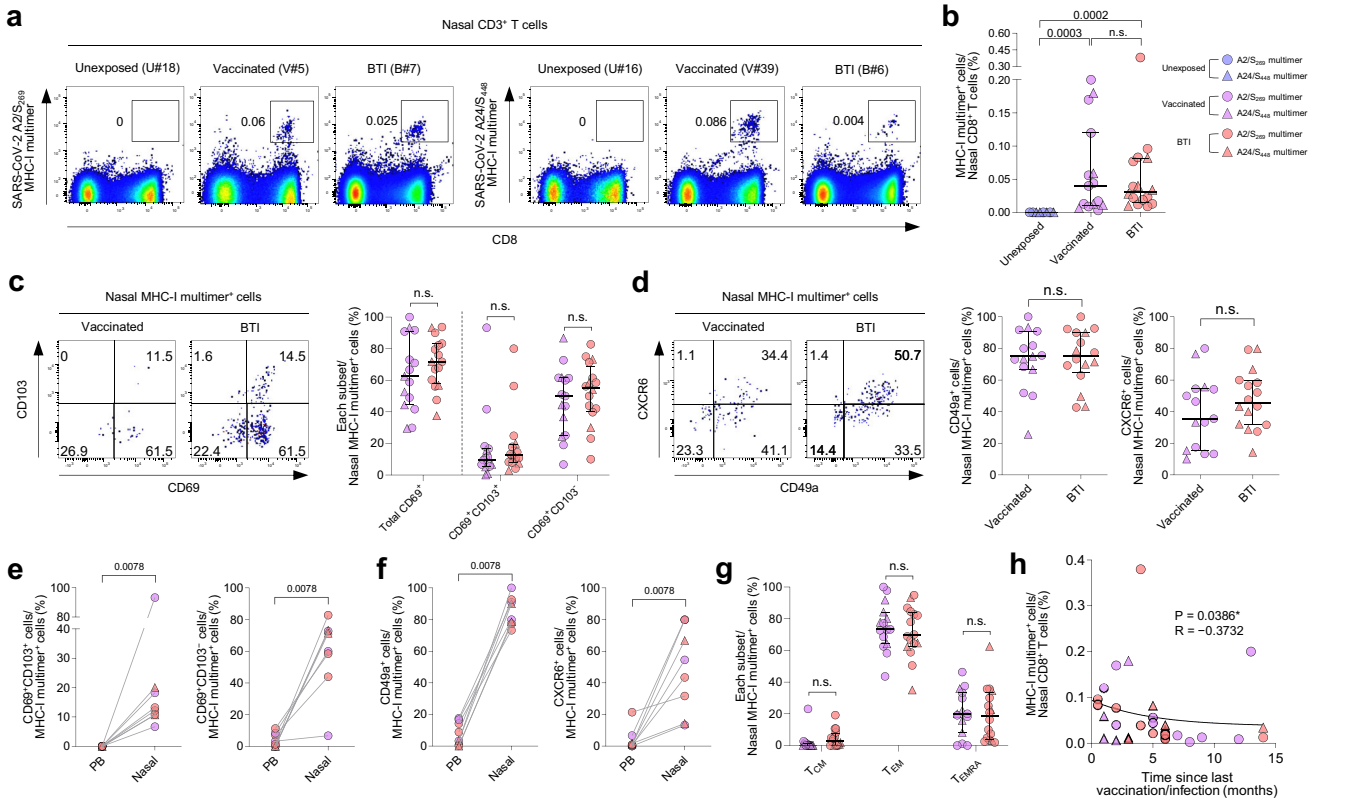

Fig. 4 | Phenotypes of S-specific nasal MHC-I multimer$^+$CD8$^+$ T cells in vaccinees without infection or with BTI. **a**–**d**, **g**, **h** Nasal cells from unexposed individuals ($n = 8$), vaccinees without infection ($n = 15$), and vaccinees with BTI ($n = 16$) were analyzed by flow cytometry. **a** Representative flow cytometry plots show ex vivo detection of SARS-CoV-2 S_{269} multimer$^+$CD8$^+$ T cells from HLA-A*02(+) individuals, and SARS-CoV-2 S_{448} multimer$^+$CD8$^+$ T cells from HLA-A*24(+) individuals in the gate of CD3$^+$ T cells. **b**, Frequency of MHC-I multimer$^+$ cells among CD8$^+$ T cells. **c**, **d** Frequencies of total CD69$^+$ (**c**), CD69$^+$CD103$^+$ (**c**), CD69$^+$CD103$^-$ (**c**), CD49a$^+$ (**d**), and CXCR6$^+$ (**d**) cells among MHC-I multimer$^+$ cells. **e**, **f** Proportions of CD69$^+$CD103$^+$ (**e**), CD69$^+$CD103$^-$ (**e**), CD49a$^+$ (**f**), and CXCR6$^+$ (**f**) cells among MHC-I multimer$^+$ cells from paired PBMCs and nasal cells, from vaccinees without infection ($n = 3$) and with BTI ($n = 5$). **g** Percentages of CCR7$^-$CD45RA$^-$ (T_{EM}), CCR7$^+$CD45RA$^-$ (T_{CM}), and CCR7$^-$CD45RA$^+$ (T_{EMRA}) cells among MHC-I multimer$^+$ cells. **h** Relationship between frequency of MHC-I multimer$^+$ cells among CD8$^+$ T cells and time since last vaccination or BTI. Solid curve is fitted to a one-phase decay model in GraphPad Prism. Data are presented as median and interquartile range. Statistical analysis was performed using the Kruskal-Wallis test with Dunn's multiple comparisons test (**b**), two-tailed Mann–Whitney U test (**c**, **d**, **g**), two-tailed Wilcoxon signed-rank test (**e**, **f**) or two-tailed Spearman's rank correlation test (**h**). n.s., not significant. Source data are provided as a Source Data file.

not significantly differ between CD49a$^+$ and CD49a$^-$ subpopulations of multimer$^+$CD8$^+$ T cells (Supplementary Fig. 9b).

CITE-seq analysis of nasal S-reactive AIM$^+$CD8$^+$ T cells confirms the enhanced effector function of the CD49a$^+$ cell subset

Finally, we performed cellular indexing of transcriptomes and epitopes (CITE)-seq analysis. SARS-CoV-2 S-reactive T cells were enriched from nasal cells of the vaccinated and BTI groups, by isolating AIM$^+$ (CD137$^+$) T cells following stimulation with S OLPs. Next, these cells were stained with DNA-barcoded antibodies against CD markers, and CITE-seq analysis was performed (Fig. 6a). After initial quality control, we used unsupervised clustering to identify CD8$^+$ T cells from total cells (Figs. 6b, c, Supplementary Fig. 10a). We further gated CD49a$^+$ cells and CD49a$^-$ cells among total CD8$^+$ T cells, based on expression levels of CD8 protein and the *ITGA1* transcript (which encodes CD49a) (Fig. 6d). We compared expression levels of effector molecule genes between CD49a$^+$ and CD49a$^-$ cells, and found that expression levels of the *IFNG*, *PRF1*, and *GZMB* transcripts were significantly higher in CD49a$^+$ cells than in CD49a$^-$ cells (Fig. 6e). These findings corroborated the results of our functional assays on nasal multimer$^+$ T cells.

Discussion

In the present study, we examined the phenotypes and functions of SARS-CoV-2 S-specific nasal T cells obtained from vaccinees with BTI or without infection. We performed MHC-I multimer staining to analyze S-specific CD8$^+$ T cells that had been primed by SARS-CoV-2 infection or vaccination. In both vaccinees with BTI and vaccinees without infection, nasal multimer$^+$CD8$^+$ T cells exhibited increased expressions of T_{RM} markers, including CD69, CD103, CD49a, and CXCR6, and exerted immediate effector functions. In particular, nasal-resident CD49a$^+$CD8$^+$ memory T cells exhibited enhanced IFN-γ production, among all vaccinees regardless of infection history. Considering that many people have been exposed to SARS-CoV-2 S antigen through vaccination or infection, our current results indicate that their nasal T_{RM} cells are capable of exerting rapid effector functions and thereby contributing to protective immunity against infection or reinfection.

Traditional cell surface markers that distinguish T_{RM} cells from circulating memory T cells include CD69 (a downmodulator of S1PR1) and CD103 (the α_E subunit of the $\alpha_E\beta_7$ integrin that binds E-cadherin)[10–12]. Since CD103 expression in T_{RM} cells depends on tissue location[35], CD69$^+$CD103$^+$ or CD69$^+$CD103$^-$ is considered a canonical phenotype of T_{RM} cells in humans. In addition to these markers, T_{RM} cells highly express CD49a, CXCR6, and CD101[11,36]. Our present results showed that CD49a marks nasal-resident CD8$^+$ memory T cells that are poised for enhanced IFN-γ production. These findings are in line with a previous report that CD49a$^+$CD8$^+$ T cells in the lungs following influenza infection have increased effector potential compared to CD49a$^-$ counterparts[37]. Similarly, in human skin, CD49a expression defines a subset of T_{RM} cells that exhibit enhanced IFN-γ production and cytotoxic phenotypes[38].

https://doi.org/10.1038/s41467-024-52689-5

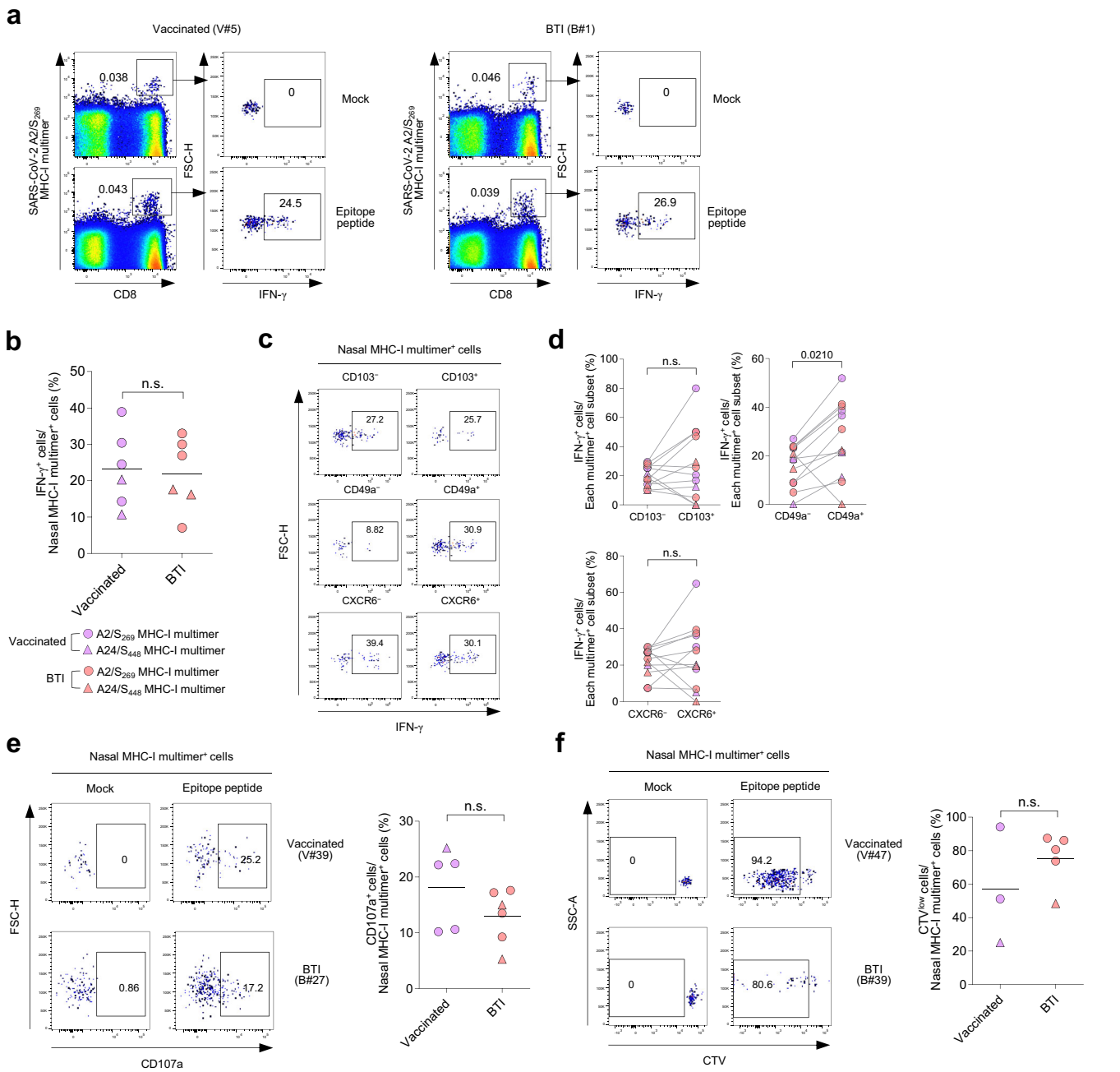

Fig. 5 | Functional analyses of S-specific nasal MHC-I multimer$^+$CD8$^+$ T cells in vaccinees without infection or with BTI. a–d Nasal cells from vaccinees without infection ($n = 6$) or with BTI ($n = 6$) were stimulated with S_{269} or S_{448} peptide (1 μg/mL) for 5.5 hours, and cytokine secretion assays and MHC-I multimer staining were performed. Representative flow cytometry plots (**a**) and summary data (**b**) showing the frequency of IFN-γ$^+$ cells among MHC-I multimer$^+$ cells. **c**, **d** Representative flow cytometry plots (**c**) and summary data (**d**) showing the frequency of IFN-γ$^+$ cells among the indicated subsets of MHC-I multimer$^+$ cells. **e** Nasal cells from vaccinees without infection ($n = 5$) and with BTI ($n = 6$) were stimulated with SARS-CoV-2 S_{269} or S_{448} peptide (1 μg/mL) for 6 hours with anti-CD107a antibody. Frequency of CD107a$^+$ cells among MHC-I multimer$^+$ cells. **f** CTV-labeled nasal cells from vaccinees without infection ($n = 3$) and with BTI ($n = 5$) were stimulated with SARS-CoV-2 S_{269} or S_{448} peptide (5 μg/mL) for 5 days. FACS plots show the frequency of CTV^{low} cells among MHC-I multimer$^+$ cells. The horizontal lines indicate the mean. Statistical analysis was performed using the two-tailed Mann–Whitney U test (**b**, **e**, **f**) or two-tailed Wilcoxon signed-rank test (**d**). n.s., not significant. Source data are provided as a Source Data file.

We confirmed the enhanced effector function of CD49a$^+$CD8$^+$ T cells compared to CD49a$^-$CD8$^+$ T cells by performing CITE-seq analysis on nasal S-reactive AIM$^+$ T cells. In the CITE-seq analysis, CD49a$^+$CD8$^+$ T cells exhibited significantly higher expression levels of the *IFNG*, *PRF1*, and *GZMB* transcripts than CD49$^-$CD8$^+$ T cells. We also found that a considerable proportion of nasal S-reactive AIM$^+$ T cells belonged to the regulatory T (Treg) cell population, including Treg (1) and Treg (2) clusters, in the CITE-seq analysis. The Treg (1) and Treg (2) clusters expressed high transcript levels of *FoxP3*, *IL2RA* (which encodes CD25), and *CTLA4*, as well as high protein levels of CD25 and CD39 (Supplementary Fig. 10a). Additionally, the Treg (1) and Treg (2) clusters exhibited significant enrichment of the Treg-specific gene set[39] compared to other T-cell clusters (Supplementary Fig. 10b). Further analysis is necessary to examine a role of nasal tissue Treg cells in SARS-CoV-2-specific responses of nasal T_{RM} cells.

Given the critical role of localized T-cell immunity against invading viruses, the induction of virus-specific T_{RM} cells by vaccination is considered an important determinant of protective

https://doi.org/10.1038/s41467-024-52689-5

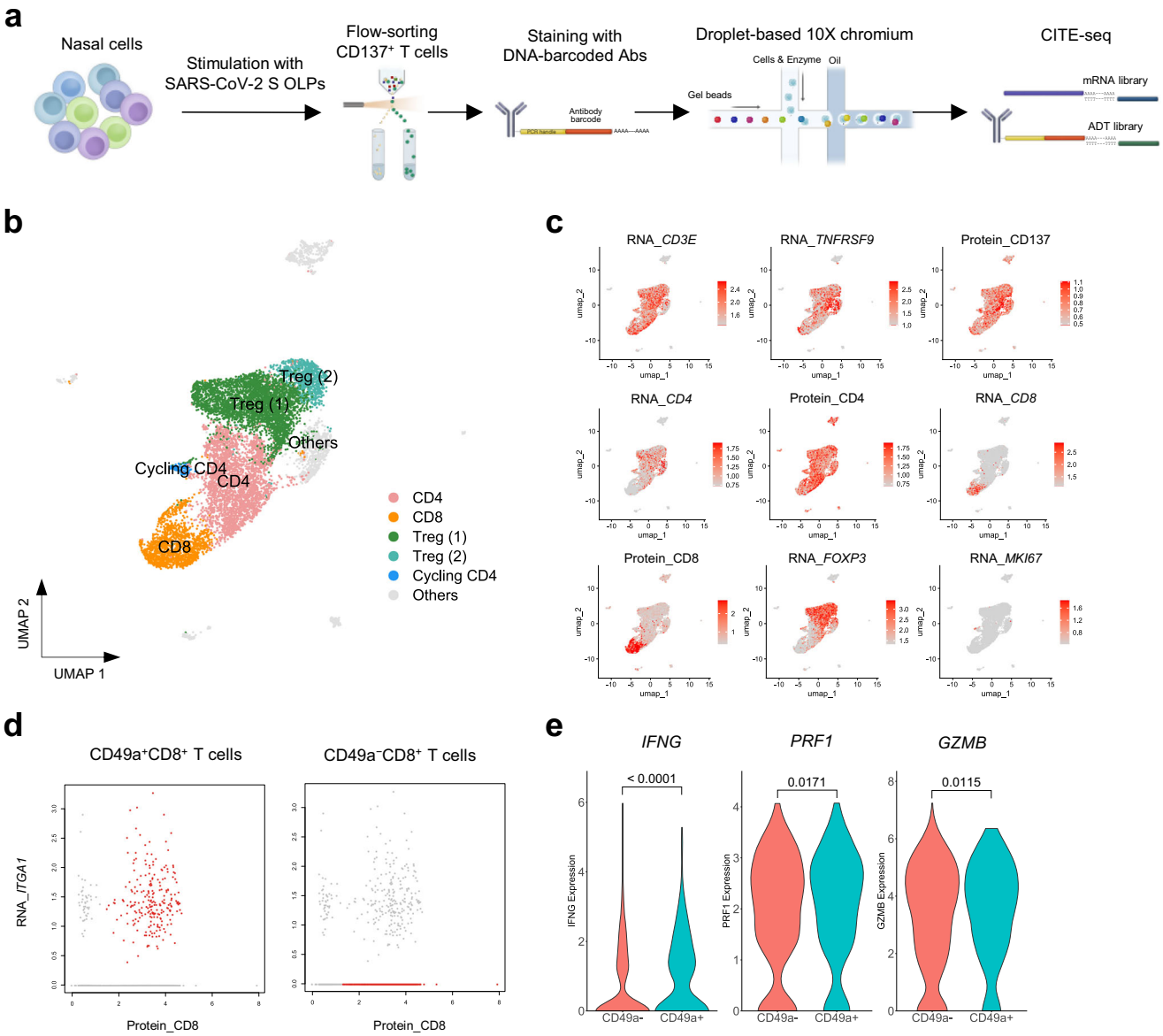

Fig. 6 | CITE-seq analyses of S-specific AIM⁺ T cells. a Summary of the experimental design (**b**) UMAP projections of 10,003 CD137⁺ T cells from vaccinees without infection ($n = 4$) and with BTI ($n = 5$), colored according to each cell type. **c** Feature plots showing the average normalized expressions of marker genes and ADTs in each cell cluster. **d** Gating strategy to identify the CD49a⁺CD8⁺ and CD49a⁻CD8⁺ T-cell subsets based on expression levels of *ITGA1* transcripts and CD8 protein. Red dots indicate each subset. **e** Violin plots showing gene expression levels among the CD49a⁺CD8⁺ and CD49a⁻CD8⁺ T-cell subsets. Statistical analysis was performed using the Mann–Whitney U test (**e**).

immunity against viral infection. Previous studies have performed ex vivo stimulation-based assays to examine the presence of SARS-CoV-2-reactive T cells in samples from the airways of vaccinees. One analysis of paired PB and BALF samples from vaccinated individuals without BTI revealed a significantly lower frequency of S-reactive T cells in BALF compared to PB[22]. In another study, nasal swab samples were analyzed, and SARS-CoV-2-reactive T cells were not detected in the nasal secretion of vaccinees without infection history[21]. That result is contradictory to our present results, which may be explained by the difference in sample types. A nasal swab collects only the fluid lining the epithelial surface, and thus the sample may include only T cells located in the epithelium and not those from the sub-epithelial compartment[40,41]. In contrast, here we analyzed surgically removed nasal tissue samples. Given that E-cadherin is a cell-cell junction protein and a classical marker of epithelial cells, T cells expressing CD103 (the α_E subunit of the $\alpha_E\beta_7$ integrin that binds E-cadherin) are preferentially located near the epithelium[42]. However, we observed that a considerable proportion of SARS-CoV-2-specific MHC-I multimer⁺ T cells did not express CD103, suggesting that a majority of SARS-CoV-2-specific CD8⁺ T cells were localized in the sub-epithelial compartment of the nasal tissue. Future studies are needed to investigate the extent to which SARS-CoV-2-specific CD103⁻CD8⁺ T cells confer protection.

A recent study using a mouse model indicates that intramuscular vaccination induces T_{RM} cells in the respiratory tract. This study revealed that intramuscular immunization with an influenza mRNA vaccine elicits bona fide influenza-specific CD8⁺ T_{RM} cells in the lungs although intranasal vaccination more effectively established lung T_{RM} cells[20]. Parabiosis experiments demonstrated that after intramuscular immunization, the majority (95–100%) of CD69⁺CD103⁻ and CD69⁺CD103⁺ cells among influenza-specific CD8⁺ T cells in the lung parenchyma were tissue-resident[20]. These results imply that intramuscular immunization alone is capable of establishing T_{RM} cells in the respiratory tract.

Ex vivo stimulation of T cells using OLPs is a useful technique for determining the total T-cell responses to a certain viral protein; however, it can potentially stimulate cross-reactive T cells. In fact, we observed S-reactive AIM$^+$ T cells among nasal cells from unexposed individuals, which may have been induced by previous infections with cross-reactive CCCoVs or animal CoVs[25–28]. Additionally, other studies have reported the presence of SARS-CoV-2 cross-reactive T cells with tissue-resident phenotypes in the pharyngeal tonsils and BALF of unexposed individuals[43,44]. To analyze CD8$^+$ T cells that were specific to SARS-CoV-2 in the nasal tissue of vaccinees, we used MHC-I multimers loaded with epitope peptides having a low degree of homology to CCCoVs[29]. This experiment confirmed the absence of multimer$^+$ cells in nasal tissue samples from the unexposed group. MHC-I multimer staining yielded the detection of multimer$^+$CD8$^+$ T cells expressing tissue-resident markers among nasal cells from vaccinees without infection, as well as vaccines with BTI. This demonstrated that intramuscular COVID-19 vaccination elicits S-specific CD8$^+$ T_{RM} cells in nasal tissues, even without SARS-CoV-2 infection. No previous study has performed MHC-I multimer staining for the detection of SARS-CoV-2-specific T_{RM} cells in human airway tissues.

Although we found functional SARS-CoV-2-specific T_{RM} cells in the nasal tissue of vaccinees without infection, further studies are needed to elucidate the precise mechanism underlying the induction of S-specific nasal T_{RM} cells in the absence of local antigens. A previous study demonstrated that T-cell migration is dynamic during the early effector phase, enabling the homing of early effector T cells to tissues beyond the original site of challenge, and subsequent differentiation into long-lived memory cells in situ[45]. Our present results may also be supported by a previous finding showing that local antigen recognition was not required for nasal T_{RM}-cell development after influenza infection[13]. Additional research is required to identify factors that affect and regulate the generation of vaccine-induced T_{RM} cells in the airway mucosa.

In summary, our current analysis demonstrates that SARS-CoV-2 S-specific CD8$^+$ T_{RM} cells are present in the nasal tissue following SARS-CoV-2 vaccination with or without BTI. Additionally, we showed that S-specific CD8$^+$ T_{RM} cells, especially the CD49a-expressing subset, exerted immediate effector functions upon antigen encounter. Since T_{RM} cells act as cardinal sentinels against viral infections, our present study enhances our understanding of the immunological effects of current vaccinations, which will serve as a basis for the development of next-generation vaccines against respiratory pathogens.

Methods

Study design

For this study, we enrolled 111 patients who underwent ESS for the treatment of sinonasal diseases at Severance Hospital, Seoul, Republic of Korea, from July 2021 to January 2024. Nasal tissue and/or PB samples were obtained from these patients. All enrolled patients had been immunized with BNT162b2 (Pfizer–BioNTech), mRNA-1273 (Moderna), ChAdOx1 nCoV-19 (AstraZeneca), Ad26COV2.S (Janssen), or NVX-CoV2373 (Novavax) prior to ESS, and had no history of SARS-CoV-2 natural infection before vaccination. The patients were categorized into two groups: vaccinees without previous infection or BTI (vaccinated group; $n = 72$) and vaccinees who experienced BTI (BTI group; $n = 39$). Individuals in the BTI group experienced BTI between March 2022 and September 2023. To confirm the absence of previous infection and BTI in the vaccinated group, we measured plasma anti-N antibody using the Elecsys Anti-SARS-CoV-2 assay (Roche Diagnostics, Indianapolis, IN, USA), which accurately detects past SARS-CoV-2 infections with 92% positivity for anti-N antibody at 18 months post-infection[46]. Individuals with a positive result on the plasma anti-N antibody assay were excluded from this study. We also obtained cryopreserved nasal cells from patients ($n = 48$) who had undergone ESS at Chungnam National University Hospital before the COVID-19 pandemic (from August 2018 to October 2019). Patients were excluded if they had used systemic or topical corticosteroids within a month before tissue collection, or had used biologicals or immunosuppressive agents. This study was conducted according to the principles of the Declaration of Helsinki, and was reviewed and approved by the institutional review boards of Severance Hospital (no. 4-2021-0573) and Chungnam National University Hospital (2018-12-025). Informed consent was obtained from all donors or from a legally authorized representative for participants under the age of 18.

Supplementary Table 1 presents the demographic and clinical characteristics of the enrolled patients. Supplementary Table 2 shows detailed information regarding the characteristics of each patient.

PBMCs were isolated by density gradient centrifugation using Lymphocyte Separation Medium (Corning, NY, USA). For nasal cell isolation, nasal tissue was mechanically dissociated, and then single-cell suspensions were prepared using a Tumor Dissociation Kit (Miltenyi Biotec, Auburn, CA, USA) with a gentleMACS dissociator (Miltenyi Biotec) and 70 μm cell strainers (SPL Life Sciences, Gyeonggido, Korea). After isolation, the cells were cryopreserved in fetal bovine serum (Corning) with 10 % dimethyl sulfoxide (Sigma-Aldrich, St Louis, MO, USA) until use.

Multi-color flow cytometry

PBMCs and nasal cells ($0.5–2 \times 10^6$) were stained with fluorochrome-conjugated antibodies against specific surface markers, for 10 min at room temperature. Dead cells were excluded using LIVE/DEAD near-IR fluorescent reactive dye (Invitrogen, Carlsbad, CA, USA). Multi-color flow cytometry was performed using a Fortessa or Lyric instrument (BD Biosciences, San Jose, CA, USA), and the data were analyzed with FlowJo software (FlowJo LLC, Ashland, OR, USA). We used the following fluorochrome-conjugated monoclonal antibodies (all from BD Biosciences): anti-CXCR6 BV421 (1:100 dilution, clone 13B 1E5, catalog no. 566007); anti-CD137 BV421 (1:100 dilution, clone 4B4-1, catalog no. 564091); anti-CD3 BV510 (1:100 dilution, clone UCHT1, catalog no. 563109); anti-CD8 BV605 (1:100 dilution, clone SK1, catalog no. 564116); anti-CXCR6 BV786 (1:100 dilution, clone 13B 1E5, catalog no. 743602); anti-CD69 BV786 (1:100 dilution, clone FN50, catalog no. 563834); anti-CD45RA BB515 (1:100 dilution, clone HI100, catalog no. 564552); anti-CCR7 PerCP-Cy5.5 (1:100 dilution, clone 150503, catalog no. 561144); anti-CD69 PE-CF594 (1:100 dilution, clone FN50, catalog no. 562617); anti-CD25 PE-Cy7 (1:100 dilution, clone M-A25, catalog no. 561405); anti-CD103 APC (1:100 dilution, clone Ber-ACT8, catalog no. 563883); anti-CD4 Alexa Fluor 700 (1:100 dilution, clone RPA-T4, catalog no. 557922); anti-CD14 APC-Cy7 (1:100 dilution, clone MφP9, catalog no. 557831); and anti-CD19 APC-Cy7 (1:100 dilution, clone SJ25C1, catalog no. 557791). We also used the following antibodies (obtained from BioLegend, San Diego, CA, USA): anti-OX40 BV711 (1:100 dilution, clone Ber-ACT35, catalog no. 350030); anti-CD103 PE (1:100 dilution, clone Ber-ACT8, catalog no. 350206); anti-CCR7 PE (1:100 dilution, clone G043H7, catalog no. 353204); and anti-CD49a PE-Cy7 (1:100 dilution, clone TS2/7, catalog no. 328312).

Activation-induced marker assay

PBMCs and nasal cells (1×10^6) were cultured for 24 hours in the presence of 1 μg/mL peptide pools, and 1 μg/mL anti-human CD28 and CD49d mAbs (BD Biosciences). Stimulation was performed using SARS-CoV-2 S OLP pools (PepTivator®, SARS-CoV-2 Prot_S Complete; Miltenyi Biotec) and N OLP pools (PepMix™ SARS-CoV-2 NCAP; JPT Peptide Technologies, Berlin, Germany). CD25$^+$CD137$^+$ cells and OX40$^+$CD137$^+$ cells were considered S-specific AIM$^+$ cells among CD8$^+$ and CD4$^+$ T cells, respectively. Negative controls were treated with DMSO and anti-CD28/anti-CD49d without peptides, and positive controls with PMA/ionomycin. The frequency of AIM$^+$ T cells was measured as background (negative control)-subtracted data. A positive response was defined as when the percentage of AIM$^+$ cells after S

OLP stimulation was at least three-fold higher than the percentage in the negative controls.

MHC-I multimer staining

PBMCs and nasal cells ($1–4 \times 10^6$) were pre-treated for 10 minutes with FcR Blocking Reagent (Miltenyi Biotec), and then stained with APC-conjugated MHC-I multimers, for 15 minutes at room temperature, and washed twice. The APC-conjugated MHC-I multimers used in this study were YLQPRTFLL (SARS-CoV-2 S_{269}) HLA-A*0201 pentamer and NYNYLYRLF (SARS-CoV-2 S_{448}) HLA-A*2402 pentamer (Proimmune, Oxford, UK). Additional surface markers were stained using the above-described protocols. Multimer$^+$ cells with a minimum count of 30 were subjected to further phenotypic and functional analyses.

Cytokine secretion assay

Nasal cells ($1–4 \times 10^6$) were stained with APC-conjugated multimers for 15 minutes at room temperature, washed, and then stimulated for 5.5 h with 1 µg/mL SARS-CoV-2 S_{269} YLQPRTFLL peptide (Mimotopes, Melbourne, Australia) or SARS-CoV-2 S_{448} NYNYLYRLF peptide (Peptron, Daejeon, Korea). Next, the cells were incubated with IFN-γ catch reagents (Miltenyi Biotec) for 55 minutes at 37 °C on a rotator, followed by staining with FITC-labeled anti-IFN-γ detection reagents (Miltenyi Biotec) for 10 minutes on ice. Additional staining was performed using APC-conjugated multimers, and antibodies for specific surface markers. This method enabled simultaneous analysis of the phenotype and function of multimer$^+$ cells although the frequency of multimer$^+$ cells among total CD8$^+$ T cells decreased after cytokine secretion assays (Supplementary Fig. 11).

CD107a degranulation assay

Nasal cells ($2 – 4 \times 10^6$) were cultured for 6 hours in the presence of 1 µg/mL epitope peptide, along with PE-conjugated anti-CD107a antibody (1:100 dilution, clone H4A3, catalog no. 555801; BD Biosciences), brefeldin A (GolgiPlug, BD Biosciences), and monensin (GolgiStop, BD Biosciences). Next, these cells were stained with MHC class I multimer and antibodies for analysis.

Proliferation assay

Nasal cells ($2–4 \times 10^6$) were stained with the cell division tracking dye CTV (Invitrogen), following the manufacturer's instructions. The CTV-labeled cells were then stimulated with 5 µg/mL epitope peptide, for 5 days of culture. Next, the cells were stained with MHC class I multimers, and proliferation was assessed by flow cytometry.

Cell sorting for CITE-seq

Nasal cells (~ 2×10^7) were stimulated for 24 h with 1 µg/mL SARS-CoV-2 S OLP pools (PepTivator®, SARS-CoV-2 Prot_S Complete; Miltenyi Biotec) and 1 µg/mL anti-human CD28 and CD49d mAbs (BD Biosciences). Subsequently, these nasal cells were stained with PE-conjugated anti-CD3 antibody (BD Biosciences), APC-conjugated CD137 antibody (Miltenyi Biotec), and LIVE/DEAD near-IR fluorescent reactive dye (Invitrogen). Finally, live CD137$^+$CD3$^+$ T cells were sorted using an ARIA II instrument (BD Biosciences).

CITE-seq analysis

Single-cell CITE-seq libraries were generated using Chromium Next GEM Single Cell 5' Reagent Kits v2 (Dual Index), in accordance with the manufacturer's instructions. The following DNA-barcoded monoclonal antibodies were used for CITE-seq (obtained from BioLegend): anti-CD107a-TotalSeq™-C (H4A3), anti-CD127-TotalSeq™-C (A019D5), anti-CD134-TotalSeq™-C (Ber-ACT35), anti-CD137-TotalSeq™-C (4B4-1), anti-CD14-TotalSeq™-C (63D3), anti-CD152-TotalSeq™-C (BNI3), anti-CD154-TotalSeq™-C (24-31), anti-CD185-TotalSeq™-C (J252D4), anti-CCR7-TotalSeq™-C (G043H7), anti-CD200-TotalSeq™-C (OX-104), anti-CD223-TotalSeq™-C (11C3C65), anti-CD25-TotalSeq™-C (BC96), anti-ICOS-TotalSeq™-C (C398.4A), anti-PD-1-TotalSeq™-C (EH12.2H7), anti-CD366-TotalSeq™-C (F38-2E2), anti-CD38-TotalSeq™-C (HIT2), anti-CD39-TotalSeq™-C (A1), anti-CD4-TotalSeq™-C (RPA-T4), anti-CD45RA-TotalSeq™-C (HI100), anti-CD57-TotalSeq™-C (QA17A04), anti-CD69-TotalSeq™-C (FN50), anti-CD8-TotalSeq™-C (SK1), anti-CD95-TotalSeq™-C (DX2), anti-HLA-DR-TotalSeq™-C (L243), anti-KLRG1-TotalSeq™-C (SA231A2), anti-TCR Vα24-Jα18-TotalSeq™-C (6B11), anti-TCR Vα7.2-TotalSeq™-C (3C10), anti-TCR α/β -TotalSeq™-C (IP26), anti-TCR γ/δ-TotalSeq™-C (B1), and anti-TIGIT-TotalSeq™-C (A15153G). Libraries were constructed and sequenced at a depth of approximately 33,000 reads per cell for gene, antibody-derived tag (ADT), and TCR sequence expression, using the Novaseq 6000 platform (Illumina, San Diego, CA, USA). The sequencing data were demultiplexed using the mkfastq function (Cell Ranger, 10X Genomics, v7.1.0) to generate fastq files. Demultiplexed fastq files of gene and ADT expression were aligned to the reference human genome (GRCH38; 10X Cell Ranger reference GRCh38-2020-A) and the barcode sequence of each ADT. Filtering, barcode counting, and UMI counting were performed to generate feature-barcode matrices using the count function (Cell Ranger, v7.1.0). These feature-barcode matrices were analyzed using the Seurat R package (Seurat, v5.1.0). For basic quality control, we filtered low-quality cells expressing mitochondrial genes in ≥ 15% of their total gene expression, < 200 genes, or > 7000 genes. We next performed standard normalization for the gene expression of each cell based on the total read count, and identified highly variable genes ($n = 2000$). The datasets were scaled (ScaleData function) and principal component analysis (PCA) (RunPCA function) carried out to dimensional reduction. Lastly, the cells underwent unsupervised clustering (FindClusters function, resolution = 0.3) and were visualized by uniform manifold approximation and projection (UMAP) using the top 25 principal components (PCs) (RunUMAP function). Within the CD8$^+$ T-cell cluster, the CD49a$^+$CD8$^+$ and CD49a$^-$CD8$^+$ T-cell subsets were selected based on the expression levels of *ITGA1* transcripts and CD8 protein (CellSelector function).

Statistical analysis

Statistical analyses were performed using GraphPad Prism version 9.1.1. for Windows (GraphPad Software, San Diego, CA, USA) and R version 4.3.3 software (R Foundation for Statistical Computing, Vienna, Austria. https://www.R-project.org/). Significance was set at $P < 0.05$. The Wilcoxon signed-rank test was used to compare data between two paired groups, and the Mann–Whitney U test to compare data between two unpaired groups. The one-way repeated-measures ANOVA with Tukey's multiple comparisons test (parametric data) was used for multiple pairwise comparisons. Additionally, the Kruskal-Wallis test with Dunn's multiple comparisons test was used to compare non-parametric data between multiple unpaired groups. The Spearman's rank correlation test or the Pearson's correlation test was used to assess the significance of correlation.

Reporting summary

Further information on research design is available in the Nature Portfolio Reporting Summary linked to this article.

Data availability

All data supporting the findings of this study are available within the main manuscript and the supplementary files or from the corresponding author upon request. All raw data for CITE-sequencing were deposited in the Gene Expression Omnibus under accession number GSE271754. Source data are provided in this paper.

Code availability

All analyses were conducted using publicly available software, as detailed in the "Methods" section. The raw scripts used to generate the

CITE-seq analysis figures presented in this paper are accessible via the Zenodo repository (https://doi.org/10.5281/zenodo.12677292).

References

1. Sekine, T. et al. Robust T cell immunity in convalescent individuals with asymptomatic or mild COVID-19. *Cell* **183**, 158–168.e14 (2020).
2. Dan, J. M. et al. Immunological memory to SARS-CoV-2 assessed for up to 8 months after infection. *Science* **371**, eabf4063 (2021).
3. Mateus, J. et al. Low-dose mRNA-1273 COVID-19 vaccine generates durable memory enhanced by cross-reactive T cells. *Science* **374**, eabj9853 (2021).
4. Sahin, U. et al. BNT162b2 vaccine induces neutralizing antibodies and poly-specific T cells in humans. *Nature* **595**, 572–577 (2021).
5. Wherry, E. J. & Barouch, D. H. T cell immunity to COVID-19 vaccines. *Science* **377**, 821–822 (2022).
6. Tarke, A. et al. SARS-CoV-2 vaccination induces immunological T cell memory able to cross-recognize variants from Alpha to Omicron. *Cell* **185**, 847–859.e11 (2022).
7. Jung, M. K. et al. BNT162b2-induced memory T cells respond to the Omicron variant with preserved polyfunctionality. *Nat. Microbiol* **7**, 909–917 (2022).
8. Gao, Y. et al. Ancestral SARS-CoV-2-specific T cells cross-recognize the Omicron variant. *Nat. Med.* **28**, 472–476 (2022).
9. McMahan, K. et al. Correlates of protection against SARS-CoV-2 in rhesus macaques. *Nature* **590**, 630–634 (2021).
10. Mueller, S. N. & Mackay, L. K. Tissue-resident memory T cells: local specialists in immune defence. *Nat. Rev. Immunol.* **16**, 79–89 (2016).
11. Szabo, P. A., Miron, M. & Farber, D. L. Location, location, location: Tissue resident memory T cells in mice and humans. *Sci. Immunol.* **4**, eaas9673 (2019).
12. Masopust, D. & Soerens, A. G. Tissue-resident T cells and other resident leukocytes. *Annu Rev. Immunol.* **37**, 521–546 (2019).
13. Pizzolla, A. et al. Resident memory CD8(+) T cells in the upper respiratory tract prevent pulmonary influenza virus infection. *Sci. Immunol.* **2**, eaam6970 (2017).
14. Kinnear, E. et al. Airway T cells protect against RSV infection in the absence of antibody. *Mucosal Immunol.* **11**, 249–256 (2018).
15. Zhao, J. et al. Airway memory CD4(+) T cells mediate protective immunity against emerging respiratory coronaviruses. *Immunity* **44**, 1379–1391 (2016).
16. Ahn, J. H. et al. Nasal ciliated cells are primary targets for SARS-CoV-2 replication in the early stage of COVID-19. *J. Clin. Invest* **131**, e148517 (2021).
17. Poon, M. M. L. et al. SARS-CoV-2 infection generates tissue-localized immunological memory in humans. *Sci. Immunol.* **6**, eabl9105 (2021).
18. Roukens, A. H. E. et al. Prolonged activation of nasal immune cell populations and development of tissue-resident SARS-CoV-2-specific CD8(+) T cell responses following COVID-19. *Nat. Immunol.* **23**, 23–32 (2022).
19. Ssemaganda, A. et al. Expansion of cytotoxic tissue-resident CD8(+) T cells and CCR6(+)CD161(+) CD4(+) T cells in the nasal mucosa following mRNA COVID-19 vaccination. *Nat. Commun.* **13**, 3357 (2022).
20. Kunzli, M. et al. Route of self-amplifying mRNA vaccination modulates the establishment of pulmonary resident memory CD8 and CD4 T cells. *Sci. Immunol.* **7**, eadd3075 (2022).
21. Lim, J. M. E. et al. SARS-CoV-2 breakthrough infection in vaccinees induces virus-specific nasal-resident CD8+ and CD4+ T cells of broad specificity. *J. Exp. Med.* **219**, e20220780 (2022).
22. Tang, J. et al. Respiratory mucosal immunity against SARS-CoV-2 after mRNA vaccination. *Sci. Immunol.* **7**, eadd4853 (2022).
23. Mitsi, E. et al. Respiratory mucosal immune memory to SARS-CoV-2 after infection and vaccination. *Nat. Commun.* **14**, 6815 (2023).
24. Carabelli, A. M. et al. SARS-CoV-2 variant biology: immune escape, transmission and fitness. *Nat. Rev. Microbiol* **21**, 162–177 (2023).
25. Grifoni, A. et al. Targets of T cell responses to SARS-CoV-2 coronavirus in humans with COVID-19 disease and unexposed individuals. *Cell* **181**, 1489–1501.e15 (2020).
26. Le Bert, N. et al. SARS-CoV-2-specific T cell immunity in cases of COVID-19 and SARS, and uninfected controls. *Nature* **584**, 457–462 (2020).
27. Nelde, A. et al. SARS-CoV-2-derived peptides define heterologous and COVID-19-induced T cell recognition. *Nat. Immunol.* **22**, 74–85 (2021).
28. Low, J. S. et al. Clonal analysis of immunodominance and cross-reactivity of the CD4 T cell response to SARS-CoV-2. *Science* **372**, 1336–1341 (2021).
29. Rha, M. S. et al. PD-1-expressing SARS-CoV-2-specific CD8(+) T cells are not exhausted, but functional in patients with COVID-19. *Immunity* **54**, 44–52.e3 (2021).
30. Wein, A. N. et al. CXCR6 regulates localization of tissue-resident memory CD8 T cells to the airways. *J. Exp. Med.* **216**, 2748–2762 (2019).
31. Rydyznski Moderbacher, C. et al. Antigen-specific adaptive immunity to SARS-CoV-2 in acute COVID-19 and associations with age and disease severity. *Cell* **183**, 996–1012.e19 (2020).
32. Jung, J. H. et al. SARS-CoV-2-specific T cell memory is sustained in COVID-19 convalescent patients for 10 months with successful development of stem cell-like memory T cells. *Nat. Commun.* **12**, 4043 (2021).
33. Rowntree, L. C. et al. SARS-CoV-2-specific CD8(+) T-cell responses and TCR signatures in the context of a prominent HLA-A*24:02 allomorph. *Immunol. Cell Biol.* **99**, 990–1000 (2021).
34. Park, S. H. et al. Successful vaccination induces multifunctional memory T-cell precursors associated with early control of hepatitis C virus. *Gastroenterology* **143**, 1048–1060.e4 (2012).
35. Kumar, B. V. et al. Human tissue-resident memory T cells are defined by core transcriptional and functional signatures in lymphoid and mucosal sites. *Cell Rep.* **20**, 2921–2934 (2017).
36. Gray, J. I. & Farber, D. L. Tissue-resident immune cells in humans. *Annu Rev. Immunol.* **40**, 195–220 (2022).
37. Reilly, E. C. et al. CD49a identifies polyfunctional memory CD8 T cell subsets that persist in the lungs after influenza infection. *Front Immunol.* **12**, 728669 (2021).
38. Cheuk, S. et al. CD49a expression defines tissue-resident CD8(+) T cells poised for cytotoxic function in human skin. *Immunity* **46**, 287–300 (2017).
39. Azizi, E. et al. Single-cell map of diverse immune phenotypes in the breast tumor microenvironment. *Cell* **174**, 1293–1308.e36 (2018).
40. Pipkorn, U. & Karlsson, G. Methods for obtaining specimens from the nasal mucosa for morphological and biochemical analysis. *Eur. Respir. J.* **1**, 856–862 (1988).
41. Ordovas-Montanes, J. et al. Allergic inflammatory memory in human respiratory epithelial progenitor cells. *Nature* **560**, 649–654 (2018).
42. Woon, H. G. et al. Compartmentalization of total and virus-specific tissue-resident memory CD8+ T cells in human lymphoid organs. *PLoS Pathog.* **12**, e1005799 (2016).
43. Niessl, J. et al. Identification of resident memory CD8(+) T cells with functional specificity for SARS-CoV-2 in unexposed oropharyngeal lymphoid tissue. *Sci. Immunol.* **6**, eabk0894 (2021).
44. Diniz, M. O. et al. Airway-resident T cells from unexposed individuals cross-recognize SARS-CoV-2. *Nat. Immunol.* **23**, 1324–1329 (2022).
45. Masopust, D. et al. Dynamic T cell migration program provides resident memory within intestinal epithelium. *J. Exp. Med.* **207**, 553–564 (2010).

46. Nakagama, Y. et al. Detecting waning serological response with commercial immunoassays: 18-Month longitudinal follow-up of anti-SARS-CoV-2 nucleocapsid antibodies. *Microbiol Spectr.* **10**, e0098622 (2022).

Acknowledgements

The authors sincerely thank Dr. Sewon Jeong for her assistance with the illustrations. This work was supported by a grant (RS-2023-00222762) from the National Research Foundation of Korea, funded by the Ministry of Science and ICT (to M.-S.R.) and a grant (HI23C1464) of the Korea Health Technology R&D Project through the Korea Health Industry Development Institute (KHIDI) funded by The Ministry of Health & Welfare, Republic of Korea (to M.-S.R.). This work was also supported by the Institute for Basic Science (IBS), Republic of Korea, under project code IBS-R801-D2 (to E.-C.S.).

Author contributions

M.-S.R., C.-H.K., and E.-C.S. designed the research. M.-S.R., Y.J., C.M.J., H.E.N., Y.M.K., H.-J.C., and C.-H.K. collected clinical specimens. M.-S.R., G.K., S.L., and J.K. performed experiments. M.-S.R., J.Y.N., C.-H.K., and E.-C.S. analyzed the results. M.-S.R., C.-H.K., and E.-C.S. wrote the manuscript.

Competing interests

The authors declare no competing interests.

Additional information

Supplementary information The online version contains supplementary material available at https://doi.org/10.1038/s41467-024-52689-5.

Correspondence and requests for materials should be addressed to Chang-Hoon Kim or Eui-Cheol Shin.

Peer review information *Nature Communications* thanks Maike Hofmann, Simon Jochems and the other, anonymous, reviewer(s) for their contribution to the peer review of this work. A peer review file is available.

[1]Department of Otorhinolaryngology, Yonsei University College of Medicine, Seoul, Republic of Korea. [2]The Airway Mucus Institute, Yonsei University College of Medicine, Severance Hospital, Seoul, Republic of Korea. [3]The Center for Viral Immunology, Korea Virus Research Institute, Institute for Basic Science, Daejeon, Republic of Korea. [4]Division of Infectious Diseases, Department of Internal Medicine, Korea University Guro Hospital, Korea University College of Medicine, Seoul, Republic of Korea. [5]Department of Otorhinolaryngology-Head and Neck Surgery, Research Institute for Medical Science, Chungnam National University School of Medicine, Daejeon, Republic of Korea. [6]Department of Medical Science, Chungnam National University School of Medicine, Daejeon, Republic of Korea. [7]Graduate School of Medical Science and Engineering, Korea Advanced Institute of Science and Technology (KAIST), Daejeon, Republic of Korea. ✉e-mail: entman@yuhs.ac; ecshin@kaist.ac.kr